IEEE Access
Multidisciplinary ⋮ Rapid Review ⋮ Open Access Journal

Received 22 September 2022, accepted 3 October 2022, date of publication 6 October 2022, date of current version 13 October 2022.

Digital Object Identifier 10.1109/ACCESS.2022.3212756

RESEARCH ARTICLE

Heavy Road Vehicle Platoon Control Considering Brake Fade With Adaptive Mass and Road Gradient Estimation

K. B. DEVIKA[1], G. ROHITH[2], AND SHANKAR C. SUBRAMANIAN[3], (Senior Member, IEEE)
[1]College of Engineering, Mathematics and Physical Sciences, University of Exeter, EX4 4QF Exeter, U.K.
[2]Orbital Astronautics, Milton Park, OX14 4SA Oxfordshire, U.K.
[3]Department of Engineering Design, IIT Madras, Chennai 600036, India

Corresponding author: K. B. Devika (d.koonthalakadu-baby@exeter.ac.uk)

ABSTRACT Heavy commercial road vehicle (HCRV) platoons are viable logistic solutions to freight movement. During long haul platoon operation, it is common to encounter roads of different gradients. This paper investigates the effect of brake fade phenomenon, which happens due to the continuous application of brake during downgrade operation on the string stability of HCRV platoons. A brake actuator model incorporating temperature effects during braking and characterizing brake fade has been used. A Sliding Mode Control (SMC) based string stable controller, which compensates for brake fade, has been designed. Since the brake fade factor and hence platoon stability directly depend upon the road gradient and vehicle mass, which are not directly measurable quantities, an algorithm that adaptively estimates the same has been integrated with the controller design. The algorithm could estimate the mass and gradient values with less than 2% mean absolute percentage error. The stability of the proposed fade compensated controller has been analyzed and its efficacy has been tested for various road conditions and for homogeneous and heterogeneous (overloaded cases) platoon operations. The proposed approach was seen to ensure string stability for all the considered test scenarios.

INDEX TERMS Brake fade, heavy commercial road vehicle, platoon, road gradient, sliding mode control, string stability.

I. INTRODUCTION

Heavy commercial road vehicle (HCRV) platoons have gained significant research interest owing to their ability to ensure efficient freight transportation [1], [2]. Autonomous HCRV platooning results in improved fuel economy, efficient utilization of available road infrastructure, less manpower requirement, and reduced greenhouse gas emissions [3], [4]. In addition to the aforementioned factors, autonomous platooning provides improved safety and better throughput from an operator's perspective. Diverse operating conditions such as road types, loading, road gradients, operating speed, and acceleration/deceleration rates would affect the stability and efficacy of long-haul platoon operations. All these factors have prompted the research community to look into multiple aspects concerning automated vehicle platooning [5], [6], [7], [8], [9].

During long-haul platoon operations, frequent application of brakes may be necessary to meet desired intervehicular distance and operating speed. Most HCRVs are equipped with friction brakes, and their continuous application would cause excessive temperature build-up in the brake system due to the friction braking process. Increasing this temperature beyond a particular critical value could result in deteriorated brake system performance, commonly known as brake fade effect [23]. Brake fade, even in one HCRV, could, in turn, degrade the platoon performance as a whole. Moreover, this effect would be more prominent for a platoon operating downhill since one must apply brakes continuously to maintain speed and avoid collisions. To the best of the authors' knowledge, state-of-the-art studies in this area are yet to incorporate the brake actuator model's temperature dynamics and study its effect on platoon

The associate editor coordinating the review of this manuscript and approving it for publication was Qi Zhou.

TABLE 1. Summary of recent research in road vehicle platooning.

S.No.	Paper	Vehicle model	Gradient	Temperature effects	Estimation scheme	Platoon type	Controller
1.	Tuchner et al. [10]	Third order + delay	✗	✗	✓	▷	Interpolating
2.	Xiao et al. [11]	Dynamic model + delay	✗	✗	✗	▷, ▶	SMC
3.	Liang et al. [12]	Dynamic model	✓	✗	✗	▷	Optimal
4.	Németh et al. [13]	Linear	✓	✗	✗	▷	H_∞
5.	Yu et al. [14]	HEV model	✓	✗	✗	▷	MPC
6.	Németh et al. [15]	Linear	✓	✗	✗	▷	LPV
7.	Zhai et al. [16]	Dynamic model	✓	✗	✗	▷	MPC
8.	Chen et al. [17]	Kinematic model	✓	✗	✗	▷	FSF
9.	Ploeg et al. [18]	Third order + delay	✗	✗	✗	▷	H_∞
10.	Guo et al. [19]	Kinematic model	✗	✗	✗	▷	SMC
11.	Dunbar et al. [20]	Kinematic model	✗	✗	✗	▷, ▶	Receding horizon
12.	Guo et al. [21]	Dynamic model	✓	✗	✗	▷	Adaptive SMC
13.	Devika et al. [22]	Dynamic model	✗	✗	✗	▷, ▶	SMC
14.	**Current study**	Dynamic model	✓	✓	✓	▷, ▶	SMC

▷ - Homogeneous platoon, ▶ - Heterogeneous platoon.

stability. In this context, this paper investigates the effects of excessive temperature build-up and the associated brake fade effect on the platoon operation. This paper also presents a controller design that would accommodate the brake fade effect for ensuring collision-free stable autonomous HCRV platooning.

During long-haul operations, if multiple HCRVs follow the same route to the same/different destinations, vehicles with different loads tend to form platoon formations en-route and disperse at unique destinations, for utilizing the advantages of plying in a platoon formation [12], [24]. In such platoon formations, there are instances where the individual mass of each HCRV would be different from one another depending upon loading conditions. Sometimes, the HCRVs are overloaded (although this may not be legal), considering short-term cost benefits. For the same speed of operation (same initial and final speed), overloading the vehicle would further increase the brake fade effect since the vehicle mass directly impacts brake system performance [23]. This aspect has also been quantitatively evaluated in this paper. The extent of brake fade also depends on the magnitude of road gradient and the time for which the brakes are continuously applied [23].

Considering the above aspects, the online availability of individual vehicle mass and road gradient information is crucial for establishing stable autonomous vehicular platoons. However, the online measurement of road gradient and vehicle mass is not straightforward using available sensors [25]. In this context, this paper uses an adaptive estimation scheme that provides online estimates of road gradient and mass [26], and it has suitably been integrated with the controller design. Further, the analysis presented in the paper found that the HCRV mass and road gradient variations could significantly affect the brake performance, and hence the platoon stability, which demonstrates the significance of an adaptive mass and gradient estimator in the controller design process.

While dealing with the practical realization of vehicle platoons and designing controllers, it is crucial to include vehicle dynamics, including resistive forces, tyre model, wheel dynamics, and brake/powertrain actuator dynamics [22]. Aspects such as pneumatic brake actuation delay and dynamics, mass variation during laden and unladen operating conditions, and dynamic load transfer during braking are critical while considering HCRV platoons. The controller design presented in this paper considers all these factors, making it a practically suitable design. Incorporating all these factors makes the HCRV platoon model nonlinear, requiring a nonlinear control strategy. Moreover, the controller should be robust enough to have a satisfactory performance under different operating conditions. In this context, a nonlinear and robust sliding mode control (SMC) technique has been used in this paper.

A qualitative summary of recent studies in this research domain and the placement of the present study are shown in Table 1. From this summary, one could observe that the state-of-the-art literature on vehicle platooning has not explicitly analyzed the effect of temperature build-up on brake system performance and the consequent effect on platoon stability. Moreover, the dependency of vehicle mass and road gradient on brake fade and platoon stability has not been given adequate attention. Also, the state-of-the-art controllers for platoon stability have not incorporated brake fade compensation to ensure stable long-haul platoon operations. Motivated by these gaps, this paper presents a heavy vehicle platoon model encompassing crucial factors such as vehicle dynamics, including resistive forces, tyre model, wheel dynamics, and brake actuator model with thermal effects, and has used this detailed model for controller design towards stable platooning.

In summary, the control objective is to design a controller for HCRV platoons using a complete vehicle dynamics

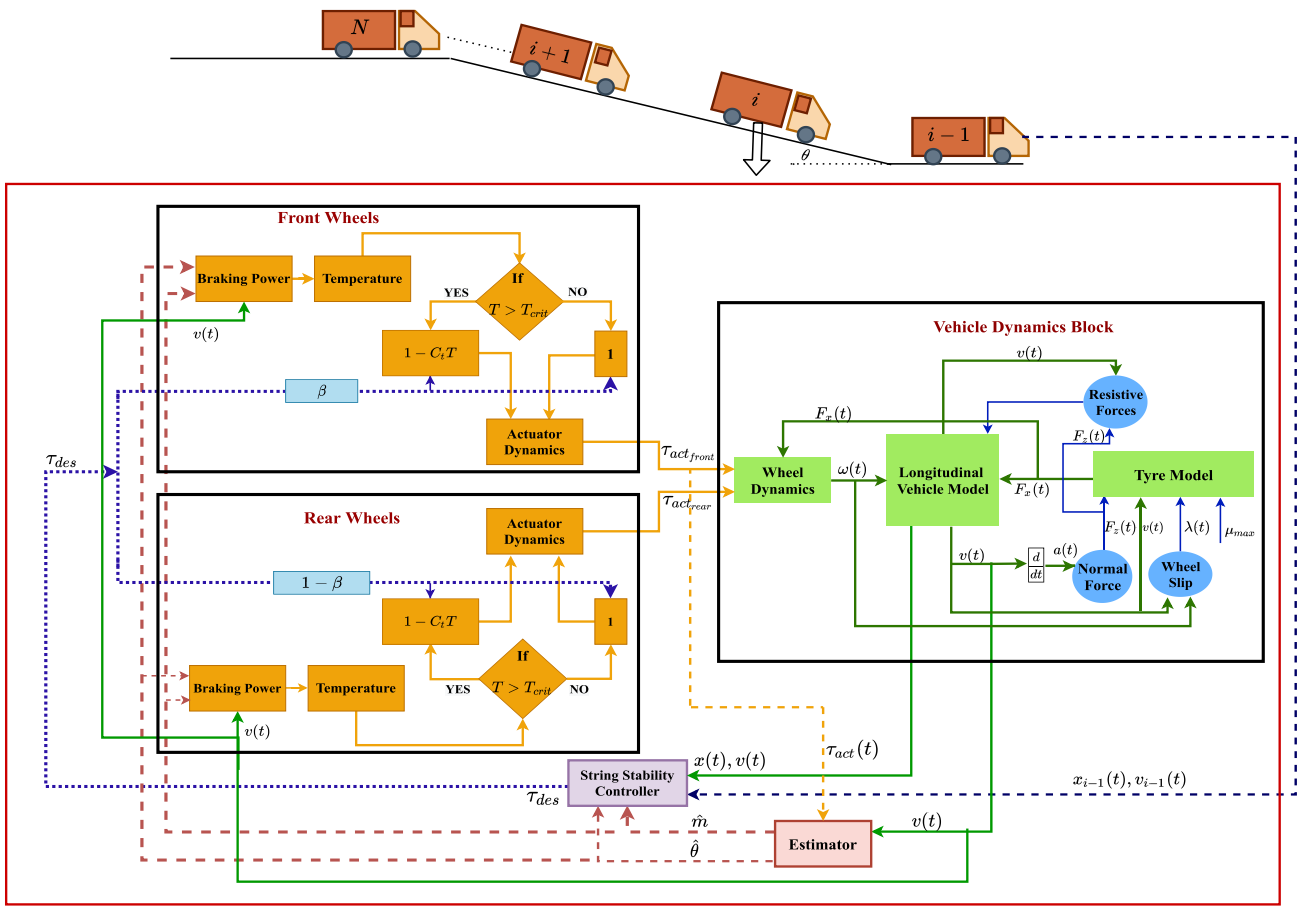

FIGURE 1. Overall block diagram (road slope θ is considered negative for downhill operation and positive for uphill operation).

model, with wheel dynamics, resistive forces, tyre model, and actuation dynamics with temperature effects to establish string stability. The controller is designed to ensure string stable platoon operation under different road and load conditions.

Based on the above discussions, the specific contributions of this paper are the following:

- A model for HCRV platoon is designed encompassing crucial factors such as vehicle dynamics including resistive forces, tyre model, wheel dynamics, and brake actuator model with thermal effects.
- A detailed investigation has been carried out on temperature build up and brake fade effect in friction brake systems during downgrade operation of HCRVs.
- Synthesis of online estimates of vehicle mass and road gradient information for string stable controller design.
- Design of a string stable controller based on SMC technique for HCRV platoons that could compensate for the brake fade effect. The controller could ensure chattering reduction, robustness and reduced reaching phase duration.
- The importance of using a dynamic model for controller design has been illustrated by comparing the controller performance with one that is based on a kinematic model.
- The significance of a modified string stable controller design incorporating brake fade effect has been presented through simulations.

II. VEHICLE MODEL

The platoon consists of $(N + 1)$ HCRVs, with one leader and N followers. The road gradient is represented by θ. In this work, only longitudinal dynamics was considered. The tyre model and vehicle parameters were assumed to be known. Equal distribution of load was assumed on the left wheel and the right wheel of the same axle. The temperature distribution was assumed uniform throughout the brake drum. The same brake parameters were used for all the HCRVs in the platoon. The driving/braking force, and longitudinal speed data were assumed to be available to estimate the road gradient and HCRV mass. The overall framework is presented in Figure 1.

A. VEHICLE MODEL

The leader HCRV can be human-driven or autonomous. It is also assumed that it can take actions independent of the rest of the HCRVs in the platoon. The following equation

characterizes the longitudinal motion of the leader vehicle:

$$\dot{x}_0(t) = v_0(t). \tag{1}$$

Here, $x_0(t)$ and $v_0(t)$ represent the position and longitudinal speed of the leader HCRV. The longitudinal speed, $v_0(t)$ is the nominal platoon speed that has to be followed by all the HCRVs for a string stable operation. The longitudinal motion of the follower HCRV is described by

$$\dot{x}_i(t) = v_i(t), \tag{2}$$

$$\dot{v}_i(t) = \frac{1}{m_i}(F_{xfi}(t) + F_{xri}(t) - F_{Ri}(t)), \tag{3}$$

where, $i = 1 \ldots N$.

Here, $x_i(t)$ and $v_i(t)$ represent the position and longitudinal speed of the i^{th} follower vehicles. $F_{xfi}(t)$ and $F_{xri}(t)$ are the brake force at the corresponding front and rear tyre-road interfaces, and m_i is the mass of the i^{th} vehicle in the platoon. The resistive force on the i^{th} vehicle is represented by $F_{Ri}(t)$, which is given by

$$F_{Ri}(t) = F_{ai}(t) + R_{xfi}(t) + R_{xri}(t) + F_{Gi}(t). \tag{4}$$

Here, $F_{ai}(t) = \frac{1}{2}\rho v_i^2(t) A_{fi} C_{di}$ is the force due to aerodynamic drag with ρ being the air density, A_{fi} representing the vehicle frontal area, and C_{di} representing the drag coefficient of the i^{th} vehicle. The gravitational force component is represented by $F_{Gi}(t) = m_i g \sin(\theta(t))$ with $\theta(t)$ representing the road slope, and R_{xfi} and R_{xri} are the forces due to rolling resistance at the front and rear wheels, respectively.

The wheel rotational dynamics are given by

$$I_{ji}\dot{\omega}_{ji}(t) = \tau_{ji}(t) - r_i F_{xji}(t), \tag{5}$$

where, $j = f, r$, represents the front and rear wheels, respectively. I_{ji} represents the wheel moments of inertia of the i^{th} vehicle, r_i is the tyre radius, $\tau_{ji}(t)$ represents the transmitted torques to the wheels.

In this study, the widely accepted Magic Formula (MF) tyre model [27] has been used. The longitudinal force as calculated using the MF tyre model is given by,

$$F_{xi}(\lambda_i(t)) = D\sin(C\arctan(B\lambda_{ix}(t) - E(B\lambda_{ix}(t) - \arctan B\lambda_{ix}(t)))) + S_V, \tag{6}$$

where, $\lambda_{ix}(t) = \lambda_i(t) + S_H$.

The MF model parameters, B, C, D, E, S_H, S_V were obtained from the vehicle dynamic simulation software, IPG TruckMaker® [28]. The variable $\lambda_i(t) = \frac{v_i(t) - r_i\,\omega_i(t)}{v_i(t)}$ represents the longitudinal slip ratio and during braking, with $\omega_i(t)$ representing angular speed of the wheel.

In a nutshell, the system model includes equations for characterizing the longitudinal dynamic response, wheel dynamics, tyre model and actuator (brake/drive) dynamics. Equation (3) represent the longitudinal dynamics of the follower vehicles, indicating the time evolution in position and speed, respectively. Equations (4), (5), and (6) represent different components in longitudinal dynamics presented in (3). Equation (4) is used to substitute for $F_{Ri}(t)$ in (3), which indicates the total resistive force acting on the i^{th} vehicle. Longitudinal forces $F_{xfi}(t)$ and $F_{xri}(t)$ are computed using the MF tyre model presented in (6). Equation (5) represents the wheel rotation dynamics that when solved, provides the wheel angular speed, which is then used to compute the longitudinal wheel slip ratio $\lambda_i(t)$. To compute the longitudinal forces at each tyre-road interface, it is imperative to have the knowledge of longitudinal slip ratio ($\lambda(t)$) for each wheel, the normal forces on the tyre and the friction coefficient (μ) between the tyres and the road [29]. The normal forces depend on factors such as total weight of the vehicle, longitudinal acceleration of the vehicle, center of gravity (C.G.) location, aerodynamic drag force and its location of action, and road inclination.

B. FRICTION BRAKE MODEL INCORPORATING BRAKE FADE EFFECT

Conventional HCRVs use pneumatic friction brake systems in which the kinetic energy is converted to thermal energy at the brake contact area [23]. The pneumatic brake actuation system in HCRVs is typically sluggish in nature, which can adversely affect the overall braking performance. In order to address the dynamics of the brake actuation system, the first order model developed by Sridhar et al. [30], has been utilized in this work. This model was calibrated using Hardware in Loop experiments and hence serves as a good approximation. The model transfer function is given by,

$$P(s) = \frac{\tau_{act}(s)}{\tau_{des}(s)} = \frac{1}{1 + \tau_d s} e^{-T_d s}, \tag{7}$$

where, τ_{des} and τ_{act} represent the demanded brake torque and actual brake torque developed. In this model, τ_d represents the brake system time constant and T_d represents the time delay. These two parameters characterizes the sluggish behaviour of pneumatic brake system. In [30], the values for τ_d and T_d have also been experimentally obtained as $\tau_d = 260$ ms and $T_d = 45$ ms, which have been utilized in this work. To mitigate the adverse effects of the pneumatic brake system delay on the closed loop stability, a lower level PID controller is integrated in to the framework [22], [31]. The details of the design procedure and analysis of the same have been presented in [22] and [31].

1) BRAKE TEMPERATURE DISTRIBUTION AND FADE FACTOR

Since friction brake systems convert the vehicle kinetic energy to heat energy, the brake temperature would increase significantly during frequent braking on downgrades resulting in brake fade. It was found that, for the fully laden ($m = 16200$ kg) HCRV plying at a constant speed of 50 km/h, if one tries to maintain the same speed during a 1 km downhill road by braking, the braking power at the end of the downhill would come down to 31% of that of the original value.

During continued downhill braking at a constant speed, braking power per brake for an individual vehicle in the platoon is given by [23],

$$P_{bi}(t) = W_i v_i(t)(\sin(\theta) - f_i) f_{bi}, \tag{8}$$

where, W_i is the vehicle weight (N), f_i is the rolling resistance coefficient, and f_{bi} is the per brake contribution [23]. The temperature developed in the brake system during braking depends on various factors like initial temperature, ambient temperature, braking power, and brake material properties. The temperature distribution per brake for an individual vehicle in a platoon (which is assumed to be uniform throughout the brake surface) during continued braking is given by [23],

$$T_i(t_b) = \left(T_{in} - T_a - \frac{P_{bi}(t)}{h_r A_r}\right) \exp\left(\frac{-h_r A_r}{\rho_r v_r c_r} t_b\right) + T_a + \frac{P_{bi}(t)}{h_r A_r}, \quad (9)$$

where, $T_i(t_b)$ represents the temperature developed during braking, t_b is the duration of brake application, T_{in} is the initial temperature, T_a represents the ambient temperature, A_r represents the drum surface area, ρ_r is the drum density, v_r is the drum volume, c_r is the drum specific heat, and h_r is the heat transfer coefficient of the drum material. The temperature developed during continuous braking varies exponentially with the braking duration and depends primarily on the braking power $P_{bi}(t)$.

This increase in brake temperature (beyond a certain value) reduces the brake effectiveness. This reduction in brake effectiveness is usually represented by using the fade factor ($f_f(t)$) and is given by [23],

$$f_f(t) = \begin{cases} 1, & T_i(t_b) \leq T_{crit}, \\ 1 - C_t T_i(t_b), & T(t_b) > T_{crit}, \end{cases} \quad (10)$$

where, T_{crit} is the critical value of temperature above which brake fade is significant, and C_t is the temperature scaling coefficient. Subsequently, the brake torque during a downhill maneuver in the presence of brake fade, $\tau_b^*(t)$ can be presented as,

$$\tau_b^*(t) = \tau_b f_f(t), \quad (11)$$

where, τ_b is the brake force without considering brake fade effects. Up to $T(t_b) = T_{crit}$, there is no considerable reduction in the brake effectiveness, as suggested by (10). Beyond this temperature, the fade factor directly indicates the loss in efficiency of the brake system.

Figure 2(a) presents the temperature developed during continuous downhill braking at different vehicle speeds for a fully laden HCRV (a fully laden mass of 16200 kg is considered) on a 10% downhill road. Brakes are applied to maintain a constant speed $v_i(t) = V_0$ in each of the considered cases. Brakes were assumed to be applied from $t_b = 0$ and the brake temperature plots are generated according to (9). The brake material properties were adopted from the literature [32], [33], and the brake design parameter values were taken from [34]. As speed increases, the vehicle's kinetic energy increases, and correspondingly the frictional heat developed also increases, as indicated by Figure 2(a). A zoomed-in version showing rapid temperature build-up for initial 5 minutes of continuous brake application is also presented in Figure 2(b). This increase in speed has an adverse effect on the braking performance, as suggested by (11). Since the fade factor is directly dependent on $T_b(t)$, the speed at which the HCRV operates has a direct impact on the loss in brake efficiency. For instance, for an HCRV descending the road at 30 km/h, if the brakes were applied continuously for 2 minutes, the fade factor value is around 0.33, and hence the actual brake torque would be only $1/3^{rd}$ of the brake torque needed to keep the vehicle at 30 km/h.

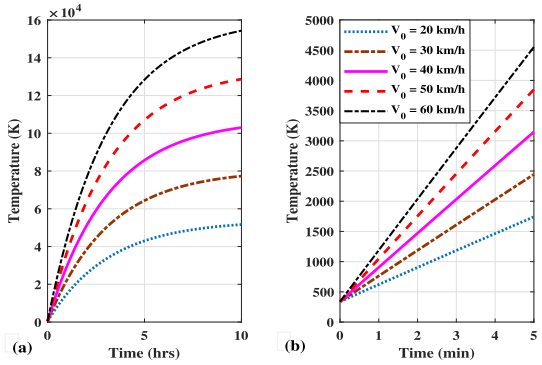

FIGURE 2. Plots of temperature vs. time during continuous downhill braking on a 10% downhill road; (a). exponential variation as per Eq. (9), (b). zoomed out profile during initial 5 mins.

Another critical factor that may affect the brake performance, and hence platoon stability, is the knowledge of the operating conditions in which the control schedules (brake torque) are generated. From (8), two important factors that affect brake performance are the HCRV mass and the road gradient. Overloading could have adverse effects on brake performance and could cause accidents. For instance, if one were to assume same speed (initial and final) during a braking procedure for a fully laden and overloaded HCRV, then the braking time for the overloaded vehicle would be higher compared to the fully laden vehicle. This would cause increased temperature build up and could adversely affect the braking process, and hence string stability.

A similar trend was visible for different gradient conditions also, where, the temperature developed would be higher for roads with higher slopes. Proper knowledge of these parameters is essential for devising a control strategy for achieving string stable platoon operation in different operating conditions. One major hurdle in realizing this aspect is the inaccessibility of the direct measurement values for both mass and road gradient. If one assumes N HCRVs to form a platoon formation en-route, different HCRVs would be of different mass, making the controller design difficult. Also, online measurement of varying road slope information is not readily available during long haul platoon operation. This motivates the estimation of both mass and road gradient, which could subsequently be used for the controller design.

C. ADAPTIVE ESTIMATION OF ROAD GRADIENT AND HCRV MASS

An adaptive estimation strategy as proposed by Yang et al. [26] has been used in this study to estimate

both HCRV mass and road gradient. In [26], the estimation scheme has been evaluated for small cars, but in this work, it has been evaluated for heavy trucks to estimate the mass of laden and unladen heavy trucks with mass values ranging from 4700 kg (unladen mass) to 22600 kg (overloaded mass). The mass estimation process is important for heavy trucks due to their significant mass variation during operation, which would impact their dynamic response and thus affect the platoon stability and performance. This method has the flexibility of estimating other vehicle parameters such as drag coefficient and rolling resistance coefficient also, in case such a need arises. To accurately estimate HCRV mass and road gradient, this scheme requires only longitudinal speed and braking force information, which can be obtained from Canbus data [25], [35], [36], and acceleration data is assumed to be obtained using accelerometer measurements. The value of $F_x(t)$ can be calculated from brake pressure measurements and that of longitudinal speed can be obtained from the wheel speed data. This method of obtaining $F_x(t)$ and $v(t)$ would not be accurate when the slip ratio becomes larger such as during panic braking and braking on low friction road surfaces. Further, the sensitivity of the estimation scheme to external noise disturbances has also been evaluated.

The longitudinal force balance equation can be rewritten as,

$$\dot{v}(t) = \Phi(v(t), F_x(t)) \cdot \Delta, \tag{12}$$

where, $\Phi(v(t), F_x(t)) = \begin{bmatrix} F_x(t) & -g & -1 & -v^2(t) \end{bmatrix}^T$ represents the regressor vector and $\Delta = \begin{bmatrix} \frac{1}{m} & \sin\theta & gf_i\cos\theta & \frac{D_a}{m} \end{bmatrix}^T$ represents the parameter vector to be estimated. The variable $F_x(t) = F_{xf}(t) + F_{xr}(t)$ represents the total longitudinal force, f_i represents the rolling friction coefficient, $D_a = \frac{1}{2}\rho A_f C_d$, and $g\sin(\theta)$ denotes the gravitational force component. The estimation steps are presented under the assumption that both $v(t)$ and $F_x(t)$ are measurable/inferrable and bounded. The main steps in the estimator design can be summarised as [26],

1) Define filtered variables $v_f(t)$ and $\Phi_f(t)$ such that,

$$\dot{v}_f(t) = \frac{1}{K_f}(v(t) - v_f(t)),$$
$$\dot{\Phi}_f(t) = \frac{1}{K_f}(\Phi(t) - \Phi_f(t)), \tag{13}$$

where, $K_f > 0$ is a constant, and $v_f(0) = \Phi_f(0) = 0$.

2) Define filtered matrix $\mathbf{M}(t)$ and vector $\mathbf{n}(t)$ such that,

$$\dot{\mathbf{M}}(t) = -L\mathbf{M}(t) + \Phi_f(t)\Phi_f^T(t),$$
$$\dot{N}(t) = -L\mathbf{n}(t) + \Phi_f(t)[(v(t) - v_f(t))/K_f], \tag{14}$$

where, $\mathbf{M}(t) \in \Re^{4\times4}$ and $n(t) \in \Re^4$, $L > 0$ is a constant, $\mathbf{M}(0) = 0$, and $n(0) = 0$.

3) Define auxiliary vector $w(t) \in \Re^4$ such that,

$$w(t) = \mathbf{M}(t)\hat{\Delta}(t) - \mathbf{n}(t), \tag{15}$$

where, $\hat{\Delta}(t)$ is the estimated value of $\Delta(t)$.

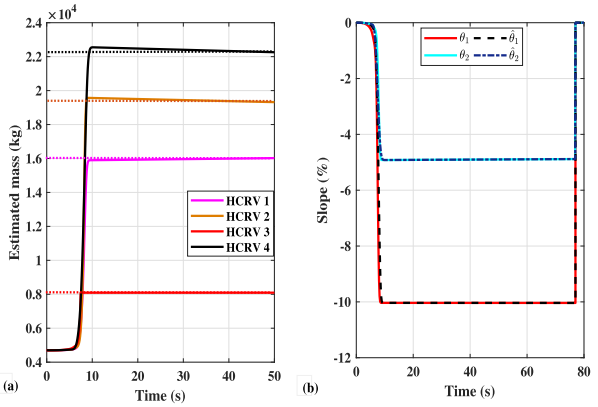

FIGURE 3. Estimation plots for mass and slope; (a). Estimated mass vs time for different loading conditions, (b). Estimated slope vs time for different road gradients.

TABLE 2. Performance evaluation of the estimation scheme.

Braking scenario	λ_{max}	MAPE$_{mass}$	MAPE$_{grade}$
$\mu = 0.8$, constant speed	0.014	1.54%	0.37%
$\mu = 0.5$, constant speed	0.016	1.80%	0.52%
$\mu = 0.4$, constant speed	0.50	2.52%	0.90%
$\mu = 0.3$, constant speed	1	–	–
$\mu = 0.8$, $d = 0.5$ m/s^2	0.035	10.15%	0.39%
$\mu = 0.8$, $d = 1$ m/s^2	0.005	21.72%	0.63%
$\mu = 0.8$, $d = 2.5$ m/s^2	0.40	27.28%	1.2%
$\mu = 0.8$, $d = 5$ m/s^2	1	–	–

4) Define estimated vector $\hat{\Delta}(t)$ as,

$$\hat{\Delta}(t) = -\Gamma\,\mathbf{w}(t), \tag{16}$$

where, $\Gamma = \text{diag}(\gamma_1, \gamma_2, \gamma_3, \gamma_4)$, with γ_1 to γ_4 taking positive values.

5) Calculate $\hat{m}(t)$, $\hat{\theta}(t)$ from $\hat{\Delta}(t)$.

In order to test the efficacy of the estimation scheme, a platoon of 4 HCRVs with different mass, $M_1 = 16200$ kg (fully laden), $M_2 = 19440$ kg (20% overloaded), $M_3 = 8100$ kg (partially laden), and $M_4 = 22600$ kg (40% overloaded), were considered. An initial value of 4700 kg, corresponding to the unladen HCRV mass, was considered. The measurements were assumed to be affected by random noise with a signal to noise ratio (SNR) value of 10 dB [37]. Figure 3(a) presents the estimated mass curves for the aforementioned HCRV platoon with different masses, with dotted lines indicating the true values. The scheme adopted could accurately estimate different mass values that could be used for the controller design. To check the accuracy of the estimation scheme, the mean absolute percentage error (MAPE) of the steady state estimates were calculated. The percentage MAPE values of M_1, M_2, M_3, and M_4 have been obtained as, 1.54%, 0.31%, 0.48%, and 0.86%, respectively. Similarly, slope estimation curves for two different downhill gradient magnitudes are presented in Figure 3(b). Two different slope values of -10% and -5% were estimated. Percentage MAPE values of 0.37% and 1.83% have been obtained for the two considered cases.

Table 2 presents the performance evaluation of the estimation scheme under different operating scenarios. The maximum slip ratio values, indicated by λ_{max} is presented for

different scenarios. The estimation scheme is tested for its efficacy in different road conditions and braking scenarios. The estimation algorithm performance was found to be deteriorated (denoted by higher MAPE magnitudes) for higher deceleration values.

III. STRING STABLE CONTROLLER WITH BRAKE FADE COMPENSATION

In a vehicle platoon, for string stable operation, all the vehicles should follow the nominal speed (typically the speed of the leader vehicle) and should also maintain a desired inter vehicular distance. Any perturbation acting on the platoon may affect these requirements and may cause spacing error propagation along the platoon, leading to string instability, which ultimately results in collision between the vehicles. In this regard, for an autonomous string stable vehicle platooning, a controller which is capable of attenuating spacing errors along the platoon is an essential requirement.

For the platoon of HCRVs under study, the spacing between a pair of vehicles is given by

$$d_i(t) = x_{i-1}(t) - x_i(t), \tag{17}$$

and the desired inter-vehicular distance is defined as

$$s_d(t) = s_o + h_i v_i(t), \tag{18}$$

where, s_o and h_i are the standstill spacing and the Constant Time-Headway (CTH), respectively.

Now, the spacing error between two consecutive vehicles can be written as

$$e_i(t) = d_i(t) - s_d(t). \tag{19}$$

Here, the control objective is to drive the spacing error to zero, such that,

$$d_i(t) \to s_o + h_i v_i(t). \tag{20}$$

On substituting $F_{xfi}(t)$ and $F_{xri}(t)$ from (5) in (3), the follower vehicle dynamics is obtained as,

$$\dot{v}_i(t) = \frac{1}{m_i}\Big[\frac{1}{r_i}(\tau_{fi}(t) - I_{fi}\dot{\omega}_{fi}(t)) + \frac{1}{r_i}(\tau_{ri}(t) - I_{ri}\dot{\omega}_{ri}(t)) - F_{Ri}(t)\Big]. \tag{21}$$

A. BRAKE MODE

During the brake mode, a linear brake torque proportion (β) between the front and rear wheels is assumed [38], such that,

$$\frac{\tau_{fi}(t)}{\tau_{ri}(t)} = \frac{\beta}{1-\beta}. \tag{22}$$

On using this linear proportion in (21),

$$\dot{v}_i(t) = \frac{1}{m_i}\Big[\frac{1}{r_i}\Big(\frac{\beta}{1-\beta}\tau_{ri}(t) - I_{fi}\dot{\omega}_{fi}(t)\Big) + \frac{1}{r_i}(\tau_{ri}(t) - I_{ri}\dot{\omega}_{ri}(t)) - F_{Ri}(t)\Big]. \tag{23}$$

Now, if one were to consider the brake fade effect, the actual torque output from the brake actuator would be considerably less than the torque required for actual safe/collision-free operation. Let $\tau^*_{fi}(t)$ and $\tau^*_{ri}(t)$ be the actual torque output from brake actuator incorporating brake fade effects such that, $\tau^*_{fi}(t) = f_f(t)\tau_{fi}(t)$ and $\tau^*_{ri}(t) = f_f(t)\tau_{ri}(t)$. Incorporating this torque reduction, (21) becomes,

$$\dot{v}_i(t) = \frac{1}{m_i}\Big[\frac{1}{r_i}(\tau^*_{fi}(t) - I_{fi}\dot{\omega}_{fi}(t)) + \frac{1}{r_i}(\tau^*_{ri}(t) - I_{ri}\dot{\omega}_{ri}(t)) - F_{Ri}(t)\Big]. \tag{24}$$

Now on applying (22) and incorporating fade factor term $f_f(t)$, (24) can be written as,

$$\dot{v}_i(t) = \frac{1}{m_i}\Big[\frac{1}{r_i}\Big(\frac{\beta}{1-\beta}f_f(t)\tau_{ri}(t) - I_{fi}\dot{\omega}_{fi}(t)\Big) + \frac{1}{r_i}(f_f(t)\tau_{ri}(t) - I_{ri}\dot{\omega}_{ri}(t)) - F_{Ri}(t)\Big]. \tag{25}$$

On rearranging the above equation,

$$\dot{v}_i(t) = \tau_{ri}(t)\Big[\frac{1}{m_i r_i}f_f(t)\Big(1 + \frac{\beta}{1-\beta}\Big)\Big] - \frac{1}{m_i r_i}\Big(I_{fi}\dot{\omega}_{fi}(t) + I_{ri}\dot{\omega}_{ri}(t)\Big) - \frac{F_{Ri}(t)}{m_i}. \tag{26}$$

Here, τ_{ri} is the control input which needs to be synthesised using SMC. For the design of SMC based control equation, the sliding function is defined as

$$s_i(t) = e_i(t) + \int_0^t \kappa e_i(\tau) d\tau. \tag{27}$$

Here, $e_i(t)$ is the intervehicular spacing error given by (19). The term, κ is the slope of the sliding function, which is a positive constant. The sliding function with an integral term is selected here in order to avoid the use of derivatives of acceleration (jerk) data from preceding vehicles. If the standard sliding function, $s_i(t) = \dot{e}_i(t) + \kappa e_i(t)$ were chosen, jerk terms would appear while obtaining the control equation by taking the first derivative of the sliding function. This additional data requirement makes the controller design complex and subsequently makes controller implementation difficult. Moreover, selecting the sliding surface with an integral term omits the need to consider the time derivative values of fade factor ($f_f(t)$) terms in the control synthesis. Computation of $\dot{f}_f$ would be challenging and would create unwanted complexities in the controller design process. The selection of a sliding surface of the form presented in (27) would avoid the need for computing $\ddot{v}_i(t)$, and thus reducing the overall controller design complexity.

The sliding function given by (27) has been defined for driving the intervehicular spacing error between two consecutive vehicles to zero. However, for string stability, the sliding function should be redefined for attenuating the spacing error

propagation [19]. For this, the sliding function is redefined as

$$S_i(t) = \begin{cases} qs_i(t) - s_{i+1}(t), & i = 1, \ldots, N-1 \\ qs_i(t), & i = N, \end{cases} \quad (28)$$

where, $q > 0$.

For designing SMC control equation, Power Rate Exponential Reaching Law (PRERL) structure has been used in this work [39]. PRERL structure is given by

$$\dot{S}_i(t) = -\frac{\psi}{\delta_0 + (1-\delta_0)e^{-\alpha|S_i(t)|^p}} |S_i(t)|^\chi \text{sign}(S_i(t)). \quad (29)$$

Here, $\psi > 0$ is the controller gain, $\delta_0 < 1, \alpha > 0, 0 < \chi < 0.5$ and $p > 0$ are controller parameters that affect the reaching time and chattering mitigation properties. On evaluating the first derivatives of (28) and (27), and using the vehicle dynamics equation given by (26) and the PRERL structure given by (29), one can write,

$$\begin{aligned} \dot{S}_i(t) &= q(v_{i-1}(t) - v_i(t)) + q\kappa e_i(t) - \dot{e}_{i+1}(t) - \kappa e_{i+1}(t) \\ &\quad -qh_i\Big[\frac{-1}{m_i r_i}\big(I_{fi}\dot{\omega}_{fi}(t) + I_{ri}\dot{\omega}_{ri}(t)\big) - \frac{F_{Ri}(t)}{m_i}\Big] \\ &\quad -qh_i\Big[\frac{1}{m_i r_i} f_f(t)\big(1 + \frac{\beta}{1-\beta}\big)\Big]u_i(t) \\ &= -\frac{\psi}{\delta_0 + (1-\delta_0)e^{-\alpha|S_i(t)|^p}} |S_i(t)|^\chi \text{sign}(S_i(t)) \\ &\quad i = 1, \ldots, N-1, \\ \dot{S}_N(t) &= q(v_{i-1}(t) - v_i(t)) + q\kappa e_N(t) \\ &\quad -qh_N\Big[\frac{-1}{m_i r_i}\big(I_{fi}\dot{\omega}_{fi}(t) + I_{ri}\dot{\omega}_{ri}(t)\big) - \frac{F_{Ri}(t)}{m_i}\Big] \\ &\quad -qh_N\Big[\frac{1}{m_i r_i} f_f(t)\big(1 + \frac{\beta}{1-\beta}\big)\Big]u_i(t) \\ &= -\frac{\psi}{\delta_0 + (1-\delta_0)e^{-\alpha|S_N(t)|^p}} |S_N(t)|^\chi \text{sign}(S_N(t)). \quad (30) \end{aligned}$$

One can obtain torque control input, $u_i(t) = \tau_{ri}(t)$ as

$$\begin{aligned} \tau_{ri}(t) &= K_{\tau i}\Big[\frac{-\psi}{\delta_0 + (1-\delta_0)e^{-\alpha|S_i(t)|^p}} |S_i(t)|^\chi \text{sign}(S_i(t)) \\ &\quad -q(v_{i-1}(t) - v_i(t)) - q\kappa e_i(t) + \dot{e}_{i+1}(t) + \kappa e_{i+1}(t) \\ &\quad +qh_i\Big[\frac{-1}{m_i r_i}\big(I_{fi}\dot{\omega}_{fi}(t) + I_{ri}\dot{\omega}_{ri}(t)\big) - \frac{F_{Ri}(t)}{m_i}\Big]\Big], \\ &\quad i = 1, \ldots, N-1, \end{aligned} \quad (31)$$

where $K_{\tau i} = \frac{-1}{qh_i\Big[\frac{1}{m_i r_i} f_f(t)\big(1+\frac{\beta}{1-\beta}\big)\Big]}$, and for the last vehicle in the platoon,

$$\begin{aligned} \tau_{rN}(t) &= K_{\tau N}\Big[\frac{-\psi}{\delta_0 + (1-\delta_0)e^{-\alpha|S_N(t)|^p}} |S_N(t)|^\chi \text{sign}(S_N(t)) \\ &\quad -q(v_{N-1}(t) - v_N(t)) - q\kappa e_i(t) \\ &\quad +qh_N\Big[\frac{-1}{m_i r_i}\big(I_{fi}\dot{\omega}_{fi}(t) + I_{ri}\dot{\omega}_{ri}(t)\big) - \frac{F_{Ri}(t)}{m_i}\Big]\Big], \end{aligned} \quad (32)$$

where $K_{\tau N} = \frac{-1}{qh_N\Big[\frac{1}{m_i r_i} f_f(t)\big(1+\frac{\beta}{1-\beta}\big)\Big]}$.

Now, using (22) the torque inputs for the front wheels can be obtained as

$$\tau_{fi}(t) = \frac{\beta}{1-\beta}\tau_{ri}(t), \quad i = 1, \ldots, N-1, \quad (33)$$

and for the last vehicle in the platoon,

$$\tau_{fN}(t) = \frac{\beta}{1-\beta}\tau_{rN}(t). \quad (34)$$

B. DRIVE MODE

In a rear wheel driven vehicle, during drive mode, $\tau_{fi}(t) = 0$, and the drive torque is applied to the rear wheel. Now, in equation (21), substituting $\tau_{fi}(t) = 0$ and following the same controller design steps as presented above, the drive torque inputs can be obtained as,

$$\begin{aligned} \tau_{ri}(t) &= \frac{-m_i r_i}{qh_i}\Big[\frac{-\psi}{\delta_0 + (1-\delta_0)e^{-\alpha|S_i(t)|^p}} |S_i(t)|^\chi \text{sign}(S_i(t)) \\ &\quad -q(v_{i-1}(t) - v_i(t)) - q\kappa e_i(t) + \dot{e}_{i+1}(t) + \kappa e_{i+1}(t) \\ &\quad +qh_i\Big[\frac{-1}{m_i r_i}\big(I_{fi}\dot{\omega}_{fi}(t) + I_{ri}\dot{\omega}_{ri}(t)\big) - \frac{F_{Ri}(t)}{m_i}\Big]\Big] \\ &\quad i = 1, \ldots, N-1, \end{aligned} \quad (35)$$

and for the last vehicle in the platoon,

$$\begin{aligned} \tau_{rN}(t) &= \frac{-m_N r_N}{qh_N} \\ &\quad \times\Big[\frac{-\psi}{\delta_0 + (1-\delta_0)e^{-\alpha|S_N(t)|^p}} |S_N(t)|^\chi \text{sign}(S_N(t)) \\ &\quad -q(v_{N-1}(t) - v_N(t)) - q\kappa e_N(t) + qh_N\Big[\frac{-1}{m_N r_i} \\ &\quad \times\big(I_{fN}\dot{\omega}_{fN}(t) + I_{rN}\dot{\omega}_{rN}(t)\big) - \frac{F_{RN}(t)}{m_N}\Big]\Big]. \end{aligned} \quad (36)$$

Proposition 1: The spacing error between two consecutive vehicles will asymptotically tends to zero in finite time, if the disturbance magnitude, $|D(t)|$ acting on an individual vehicle is within the bound given by $|D(t)| < \frac{\psi|S_i(t)|^\chi}{(\delta_0 + (1-\delta_0)e^{-\alpha|S_i(t)|^p})qh_i}$.

Proof: Consider a bounded acceleration disturbance $D(t)$ in (26) such that,

$$\begin{aligned} \dot{v}_i(t) &= \tau_{ri}(t)\Big[\frac{1}{m_i r_i} f_f(t)\big(1 + \frac{\beta}{1-\beta}\big)\Big] \\ &\quad -\frac{1}{m_i r_i}\big(I_{fi}\dot{\omega}_{fi}(t) + I_{ri}\dot{\omega}_{ri}(t)\big) - \frac{F_{Ri}(t)}{m_i} + D(t). \end{aligned} \quad (37)$$

For stability analysis, consider a Lyapunov function of the form,

$$V_i(t) = \frac{1}{2}S_i(t)^2. \quad (38)$$

Differentiating (38) and substituting control equation (31) gives,

$$\begin{aligned} \dot{V}_i(t) &= \frac{-\psi\ S_i(t)}{\delta_0 + (1-\delta_0)e^{-\alpha|S_i(t)|^p}} |S_i(t)|^\chi \text{sign}(S_i(t)) \\ &\quad -qh_i D(t) S_i(t). \end{aligned} \quad (39)$$

Now, for the bound $\frac{-\psi|S_i(t)|^{\chi}}{(\delta_0+(1-\delta_0)e^{-\alpha|S_i(t)|^p})qh_i} < D(t) < \frac{\psi|S_i(t)|^{\chi}}{(\delta_0+(1-\delta_0)e^{-\alpha|S_i(t)|^p})qh_i}$,

$$\dot{V}_i(t) = \frac{-\psi\ S_i(t)}{\delta_0+(1-\delta_0)e^{-\alpha|S_i(t)|^p}}|S_i(t)|^{\chi}\text{sign}(S_i(t)) \mp S_i(t)\frac{\psi|S_i(t)|^{\chi}}{(\delta_0+(1-\delta_0)e^{-\alpha|S_i(t)|^p})}. \quad (40)$$

For asymptotic stability, $\dot{V}_i(t) < 0, \forall\ S_i(t) \neq 0$. Now, for $S_i(t) > 0$ and $S_i(t) < 0$, (40) becomes,

$$\dot{V}_i(t) = \frac{-2\psi\ |S_i(t)|^{\chi}}{\delta_0+(1-\delta_0)e^{-\alpha|S_i(t)|^p}}S_i(t). \quad (41)$$

For the selected controller parameter set $\psi > 0, 0 < \delta_0 < 1, \alpha > 0, 0 < \chi < 0.5$ and $p > 0$, $\dot{V}_i(t)$ in (41) is always less than zero $\forall S_i(t) \neq 0$ if the disturbance $D(t)$ is with in the aforementioned bounds.

String stability in a platoon is ensured if the spacing error between a pair of vehicles gets attenuated along with the platoon in the event of any bounded perturbations/disturbances. Ideally, the sting stability controller should take care of this problem and ensure stability. However, in the event of brake fade phenomenon, the magnitude of the tolerable disturbance would be affected by the temperature developed/brake application duration. Hence, one has to design the string stable controller with brake fade compensation so that it should perform in a way not to cause any further reduction in the maximum tolerable disturbance magnitude $|D(t)|$, and the platoon should be able to operate with stability. □

Proposition 2: For a controller design without accounting for the brake fade effect, for the same set of controller parameters, the disturbance bound would become proportional to $f_f(t)$, thus limiting the robustness of the string stable controller.

Proof: A controller design without accounting for the brake fade effect could be presented by not incorporating a compensation in (24). The control equations can be derived using the same procedure presented in III as,

$$\tau_{ri}(t) = K_{\tau i}\Bigg[\frac{-\psi}{\delta_0+(1-\delta_0)e^{-\alpha|S_i(t)|^p}}|S_i(t)|^{\chi}\text{sign}(S_i(t)) - q(v_{i-1}(t)-v_i(t)) - q\kappa e_i(t) + \dot{e}_{i+1}(t) + \kappa e_{i+1}(t) + qh_i\Big[\frac{-1}{m_i r_i}\big(I_{fi}\dot{\omega}_{fi}(t)+I_{ri}\dot{\omega}_{ri}(t)\big) - \frac{F_{Ri}(t)}{m_i}\Big]\Bigg], \quad i = 1,\ldots,N-1, \quad (42)$$

where $K_{\tau i} = \frac{-1}{qh_i\left[\frac{1}{m_i r_i}\left(1+\frac{\beta}{1-\beta}\right)\right]}$, and for the last vehicle in the platoon,

Now, selecting the same Lyapunov function in (38), differentiating it, and substituting (42), the disturbance found can be obtained as,

$$|D(t)| < \frac{f_f(t)\psi\ |S_i(t)|^{\chi}}{\delta_0+(1-\delta_0)e^{-\alpha|S_i(t)|^p}qh_i}. \quad (43)$$

From the analysis, based on the sufficiency condition for Lyapunov stability, it is clear that for the considered Lyapunov function, the magnitude of disturbance does not depend on the fade factor directly, but on the controller parameters and the magnitude of the sliding function. For a fixed set of controller parameters, the value of $|D(t)|$ would remain independent of the brake fade effects, owing to the inclusion of fade factor $f_f(t)$ in the controller design to compensate for the brake fade effects. But this would not be the case if the fade factor term was not incorporated while designing the controller. From (43), one could observe the direct impact of brake fade on the disturbance magnitude. Since $0 < f_f(t) \leq 1$, and for $T > T_{crit}$, the value of $f_f(t)$ would be less than one indicating brake fade. Hence, the magnitude of the disturbance for which the platoon has a string stable operation becomes lesser as $f_f(t) \to 0$. □

Proposition 3: The presented controller design framework with sliding function (28) would ensure string stable operation for $0 < q < 1$.

Proof: Since the asymptotic stability using PRERL, which ensures $S_i(t) = 0$ in finite time has already been established, based on (28),

$$qs_i = s_{i+1}. \quad (44)$$

Now, using (27),

$$q\big(e_i(t) + \int_0^t \kappa e_i(\tau)d\tau\big) = e_{i+1}(t) + \int_0^t \kappa e_{i+1}(\tau)d\tau. \quad (45)$$

On taking Laplace transform on both sides,

$$q\big[E_i(s) + \frac{\kappa}{s}E_i(s)\big] = E_{i+1}(s) + \frac{\kappa}{s}E_{i+1}(s), \quad (46)$$

which gives the spacing error propagation transfer function [19] as,

$$G_i(s) = \frac{E_{i+1}(s)}{E_i(s)} = q. \quad (47)$$

For string stability [19],

$$\big|\big|G_i(s)\big|\big| < 1 \quad \forall\ i = 1,\ldots,N. \quad (48)$$

Hence, for string stable operation, the value of q should be selected to satisfy (48). Thus for the presented controller design framework, the string stability can be ensured by selecting the parameter range $0 < q < 1$. □

IV. RESULTS AND DISCUSSIONS

The efficacy of the presented string stable controller has been evaluated through numerical simulations. A longitudinal platoon model consisting of four HCRVs was simulated using MATLAB SIMULINK®. To have a close resemblance with real-time operating conditions, a complete vehicle dynamic model consisting of wheel dynamics, resistive forces, nonlinear MF tyre model, and actuation dynamics including temperature effects were simulated. Two different road conditions, dry (co-efficient of friction, $\mu = 0.8$) and wet (co-efficient of friction, $\mu = 0.5$) were also considered. The platoon

TABLE 3. Detailed test matrix.

Road Condition	Loading Condition	Estimation Scheme	Fade Compensated Controller	String Stability
Dry ($\mu = 0.8$)	Fully laden (all vehicles)	Not used*	No	✗
Wet ($\mu = 0.5$)	Fully laden (all vehicles)	Not used*	No	✗
Dry ($\mu = 0.8$)	Fully laden (all vehicles)	Not used*	**Yes**	✓
Wet ($\mu = 0.5$)	Fully laden (all vehicles)	Not used*	**Yes**	✓
Dry ($\mu = 0.8$)	Fully laden (all vehicles)	**Yes**	**Yes**	✓
Wet ($\mu = 0.5$)	Fully laden (all vehicles)	**Yes**	**Yes**	✓
Dry ($\mu = 0.8$)	Overloaded (vehicles 2 & 4)	No	**Yes**	✗
Wet ($\mu = 0.5$)	Overloaded (vehicles 2 & 4)	No	**Yes**	✗
Dry ($\mu = 0.8$)	Overloaded (vehicles 2 & 4)	**Yes**	**Yes**	✓
Wet ($\mu = 0.5$)	Overloaded (vehicles 2 & 4)	**Yes**	**Yes**	✓

∗ The estimation scheme is not employed since the mass is assumed to be known in these test cases.

was assumed to be operating downhill with a -10% slope at a constant speed of 50 km/h, according to the standards given by [40]. Operating conditions with both homogeneous and heterogeneous loading conditions are presented. The estimated vehicle mass and road gradient information were used for controller design. For simplicity, equal brake force/torque distribution on the front and rear wheels were considered ($\beta = 0.5$). A constant slope of -10% for a distance of 1 km was considered. A detailed simulation study with different combinations of operating conditions was considered, and the complete test matrix and corresponding string stability conditions are presented in Table 3. Without the incorporation of the fade compensated controller design, the platoon stability was compromised and collisions occurred. Even without the inclusion of an adaptive mass estimation scheme, the controller could ensure a string stable operation for a homogeneous, fully laden platoon. But there was an explicit requirement for a mass estimation scheme during heterogeneous loading conditions, and a string stable operation was achieved only after incorporating the same. The lower level PID controller has been incorporated in the design framework to track the desired torque scaled by the fade factor to compensate for pneumatic brake system dynamics. Since the fade compensated controller performed well enough and assured a string stable operation for both road conditions and the simulations results were similar for both dry and wet road scenarios, only results pertaining to $\mu = 0.8$ are presented. Other vehicle parameters used in the study are taken from [28].

A. COMPARISON WITH KINEMATIC MODEL-BASED STRING STABLE CONTROLLER

A string stable controller using PRERL based SMC strategy has been designed using the kinematic-model of the vehicle and this controller has been tested for string stability. The position of each vehicle in the platoon for the test case - fully laden HCRVs travelling downhill on a surface with $\mu = 0.8$ at a speed of 50 km/h, using the kinematic-based controller [19] is shown in Figure 4. When controller was designed using the kinematic vehicle model, it resulted in a collision, whereas the dynamics based controller avoids collision and maintains string stability. It is to be noted that both the string stable controllers were designed using the same controller parameters. Even re-tuning of the kinematic model-based controller [19] failed to achieve string stability. This comparison shows the advantage of the proposed dynamics-based string stable controller for HCRV platoons.

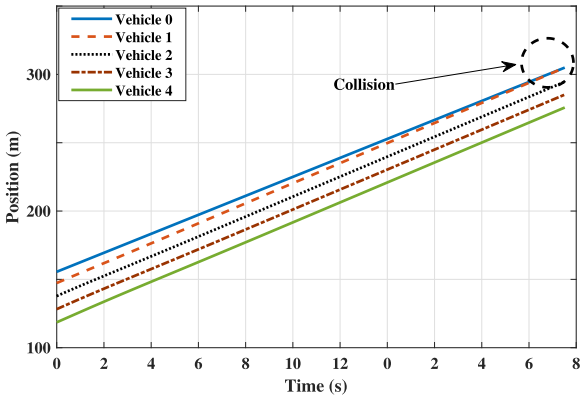

FIGURE 4. Position profile using the kinematic model-based string stable controller.

B. CHOICE OF PRERL AS THE STRING STABLE CONTROLLER

Since the primary objective is to have a collision-free string stable platoon operation, it is imperative to use a robust control method for the control of automated vehicle platoons. Even though robust, sliding mode-based controller design methodologies suffer from chattering problem, which limits the practical utility. A PEREL-based SMC design is used in this paper owing to its attributes of robustness, chattering alleviation, and finite time reachability [39]. Another common approach is to use boundary layer approaches, using sigmoid-like functions as $S_i(t)/(S_i(t) + \sigma)$ instead of signum function, for chattering alleviation [41], [42]. Such approaches have been already used for the string stable controller applications [19]. In such an approach, the value of the positive constant, σ determines the trade-off between chattering magnitude and tracking accuracy [19]. But using such an approach mitigates chattering at the cost of the SMC robustness property.

Figures 5 and 6 compare the performance of the boundary layer approach with the PRERL approach. The value of σ

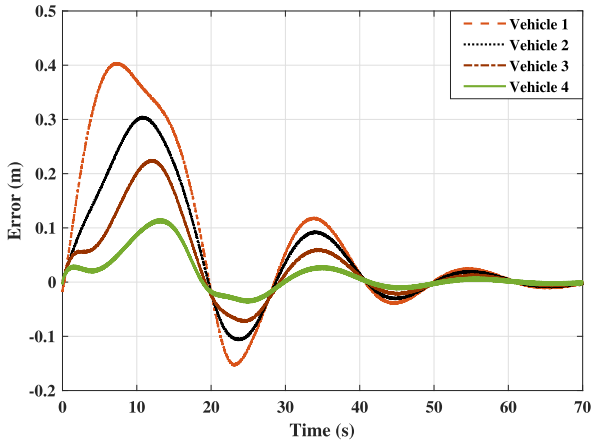

FIGURE 5. Error attenuation plots - Boundary layer method.

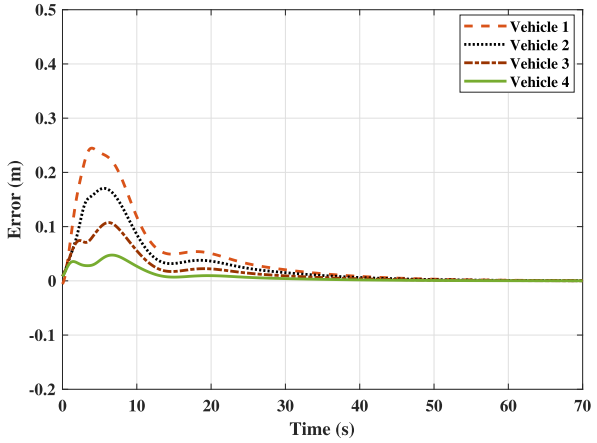

FIGURE 6. Error attenuation plots - PRERL based approach.

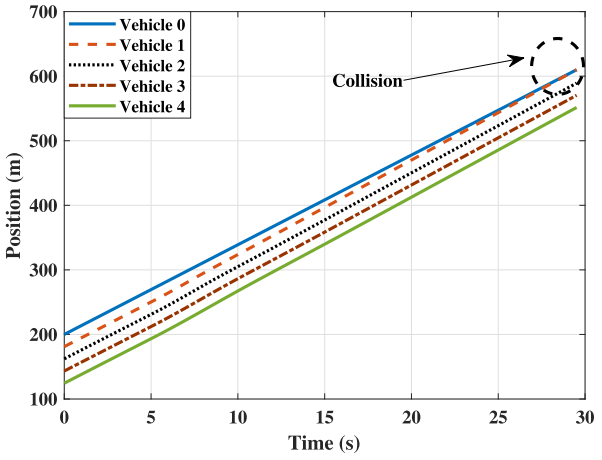

FIGURE 7. Platoon position profiles indicating collision for controller design without incorporating brake fade effect.

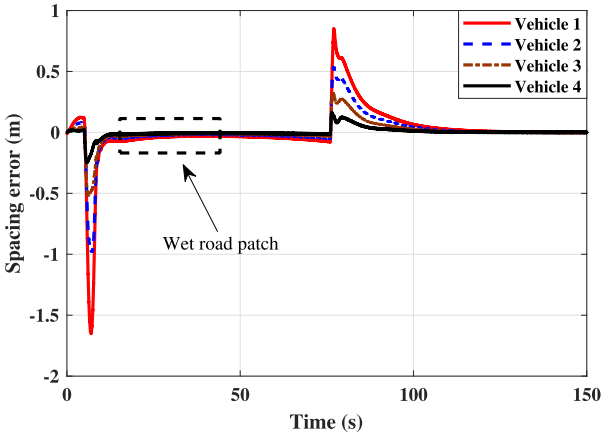

FIGURE 8. Error attenuation plots.

was chosen to be 0.1 to have finite time convergence and reduced chattering magnitude. With an initial perturbation, it was possible to attenuate the error magnitudes back to zero using both methods, but with varying transient and steady state performances. For similar control design parameters, the PRERL approach offered 40% less overshoot (for vehicle 1) and could bring the error values to zero much faster compared to that of the boundary layer approach. Also, PRERL offered a chattering free operation compared to the other method. The major drawback suffered by the boundary layer approach in terms of robustness was evident once the control structures were compared with varying slopes. In the presence of non-zero road slopes the boundary layer method was found to be inefficient in ensuring string stable platoon operations, and hence, PRERL based control design method has been adopted.

C. IMPORTANCE OF INCORPORATING BRAKE FADE EFFECT IN STRING STABLE CONTROLLER DESIGN

To understand the brake temperature effects on the platoon dynamics, initially, a controller design without incorporating the brake fade effects was considered and investigated, and the corresponding result is shown in Figure 7. For this analysis, a homogeneous fully laden (16200 kg) HCRV platoon was considered. When brake fade occurs, the brakes become less effective, and the brake actuator would provide less than the required torque during operation. Since the goal was to maintain a constant platoon speed (50 km/h) during the downhill operation, any reduction in brake torque/force would result in increased speeds and subsequent collisions. This could also be seen from Figure 7, where the leader (vehicle 0), travelling at a constant speed of 50 km/h (the leader HCRV modelled without considering any dynamics, as a kinematic model) collided with vehicle 1. Vehicle 1/HCRV 1 was modelled considering the aforementioned dynamics, and the brake fade effect in the brake actuator caused a reduction in brake torque output, and consequently, its speed increased. This resulted in a rear-end collision with the lead vehicle, and platoon instability.

Figures 8 and 9 present the spacing error attenuation profiles and speed profiles for a homogeneous HCRV platoon plying downhill with a constant speed of 50 km/h. A dry road condition with a coefficient of friction value $\mu = 0.8$ is

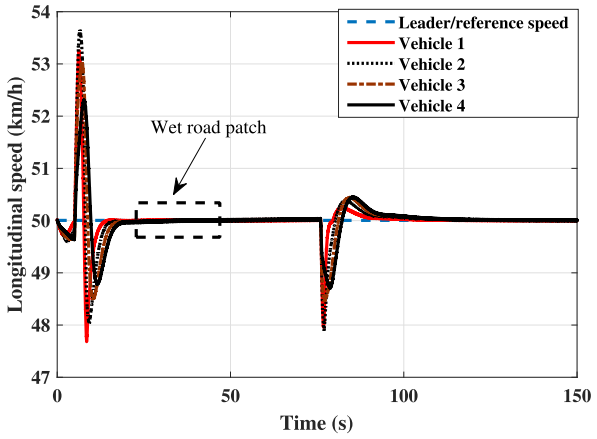

FIGURE 9. Platoon speed profiles.

considered. In order to check the robustness of the fade compensated controller to varying road conditions, a step change in μ was introduced to emulate a patch of wet road (for 200 m). The fade compensated controller was found to be robust enough to ensure stable operation without the need for controller re-tuning. The incorporation of brake fade effects in form of fade factor ($f_f(t)$) ensured a collision-free platoon operation. It was assumed that the downhill operation started at $t = 5$ s and ended at $t = 77$ s, for a length of 1 km.

The plot showing spacing error attenuation along the length of the platoon is presented in Figure 8. The initial deviation from zero value is due to the deviation in the longitudinal speed profile due to the actuator dynamics and the estimation process. The spikes in the error attenuation plot at around $t = 77$ s presented in Figure 8 is attributed to the change in road condition during downhill operation. This was also visible in the longitudinal speed profile (Figure 9) presented in the manuscript. But as one can notice, the spacing error magnitudes are getting attenuated from vehicle 1 to vehicle 4. This satisfies the notion of string stability, i.e., $\left|\frac{E(i+1)}{E(i)}\right| \leq 1$, for all vehicles in the platoon [19].

The speed profiles corresponding to the constant speed downhill maneuver is presented in Figure 9. The initial variation in longitudinal speed was due to the actuator dynamics and online estimation of mass and road gradient, as shown in Section 2.3. But this small increase/decrease in speed is not in any capacity to jeopardize the safety of the platoon operation. In a real-life situation when a driver replicates the aforesaid maneuver, there could be delays in perceiving the slope of the road, which may cause an increase/decrease in speed (according to the under/overestimation of the slope value). The pneumatic (brake) actuator delays could also play a similar role in inducing transients.

The front and rear torque profiles for string stable platoon operation incorporating brake fade effects are presented in Figure 10. Results are presented for only one vehicle (Vehicle 1) in the HCRV platoon. The fault-tolerant aspect introduced in controller design by incorporating the fade factor made the platoon string stable by computing control torque in order to compensate for the reduction in the actuator torque output. The dotted curves represent the controller output calculated according to (31) - (34). The controller output was then provided to the brake actuator with brake fade fault. Owing to the compensation provided by the controller, the attenuated brake actuator torque output (due to brake fade effect) would still be the brake torque required to keep the speed constant during the downhill maneuver, and hence maintaining a string stable platoon operation. At the end of the 1 km downhill section, the torque required to keep the platoon in string stable condition (from string stable controller) was approximately 2.57 times that of the actual actuator output, attributed to the high temperature build-up due to the continuous application of brakes. It should be noted that this demanded torque has to be well within the actuator's operating limits, characterized by the maximum pressure that can be provided by the brake actuator.

While calculating the brake torque/pressure required to maintain a string stable operation, one should also consider the constraints on the brake actuator's physical limits. For

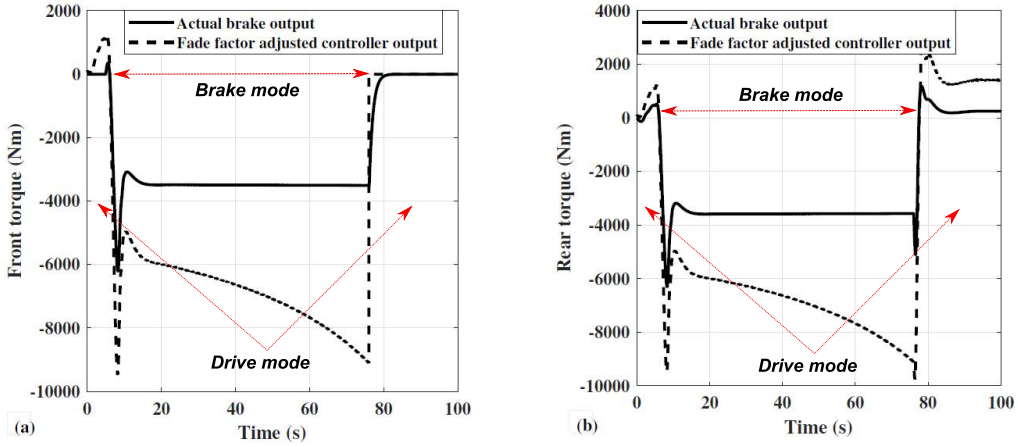

FIGURE 10. Torque profiles for stable platoon operation presented in Figures 8 and 9.

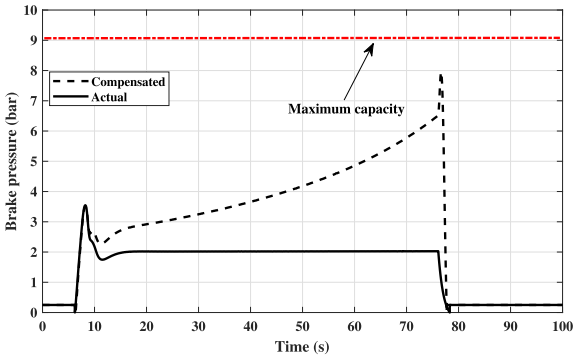

FIGURE 11. Front brake chamber pressure profiles.

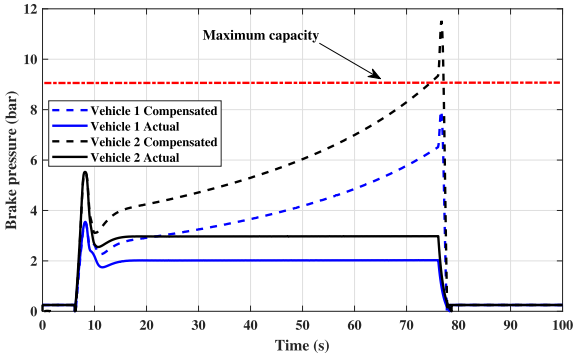

FIGURE 12. Brake pressure profiles for with heterogeneous loading conditions.

a pneumatic brake actuator, these limits are defined by the inlet pressure, contact pressure, and physical parameters of the considered actuator. If the required pressure exceeds the capacity of the actuator, then it would not provide the necessary output to keep the platoon in a string stable formation. The front brake chamber pressure profiles for the platoon operation as in Figures 8 and 9 is presented in Figure 11. The fade compensated controller demands additional pressure from the pneumatic brake system to counteract the reduction in brake effectiveness due to brake fade. In the considered scenario, the demanded pressure is well with in the maximum capacity of the actuator (for the considered pneumatic brake model, the maximum capacity is at 9 bars), and the brake actuator can meet the controller demand to compensate the brake fade. But this problem would be significant in case of longer brake application (higher temperature build-up) or overloaded cases.

D. EFFECTS OF OVERLOADING AND ROAD CONDITIONS

A scenario was also considered where there were overloaded vehicles in the platoon. Vehicles 1 and 3 were assumed to be fully loaded, and vehicles 2 and 4 were assumed to be overloaded by 40%. The plots were similar to Figures 8 and 9, and the corresponding front brake pressure profiles for HCRV 1 (fully loaded) and HCRV 2 (overloaded by 40%) are presented in Figure 12. When the vehicle is overloaded, the pressure required for a stable operation would be higher than the ideal scenario where the vehicle is fully loaded. Again, overloading would cause extra load on the mechanical systems, viz., suspensions, axles, etc., and on the brake system. This would cause a comparatively higher temperature build-up. The controller would generate torque output to compensate for this additional factor, as presented in Figure 12. But compensating the torque deficiency in this manner might not ensure a string stable operation in every scenario.

If the vehicle is overloaded, then an increase in load would result in the need for additional brake torque/pressure to slow down/keep longitudinal speed constant. This would limit the operating range (in terms of downhill distance - as distance increases, temperature increases, and hence more torque/pressure is required to compensate for the brake fade effect) compared to a fully laden scenario. The only plausible and logical solution in such scenarios would be to reduce the operating speed to lower values, so that even in presence of brake fade faults, the additional torque/pressure requirements would be well with in the physical limits of the brake actuator, and thus could be achieved to have a string stable operation. It is to be noted that the proposed SMC based string stable controller offers satisfactory performance under the presence of modelling uncertainties too. The controller ensured string stability for up to 25% modelling uncertainty magnitude in the brake fade model. Above this magnitude, the actuator saturation limits were exceeded resulting in collisions. Initially, the platoon was considered to be stable and then the lead vehicle was subjected to a speed perturbation. Under such an assumption, the proposed CTH based SMC controller resulted in string stable operation during the lead vehicle speed perturbation maneuver. However, there would be scenarios with that could result in stability issues during the initial reaching phase during real platoon operations [19]. This would be investigated as part of future research. It may be possible to address this problem using centralized/decentralized approaches as presented in [43] and [44], or distributed formation control approaches [45], [46], [47], which may provide more optimal solutions, and could be explored as future work.

V. CONCLUSION

Brake fade is one of the significant factors that compromise brake safety, especially during downhill operations. Safety/control strategies for an HCRV platoon with such a fault is rarely considered, but is of significance considering the increased demand for HCRV platoons for freight movement. In this regard, this work presented a robust control strategy based on sliding mode control for the string stable operation of HCRV platoons in the presence of brake fade fault for different operating conditions. To achieve this, a detailed HCRV platoon model incorporating wheel dynamics, nonlinear Magic Formula tyre model, resistive forces, brake actuator model, including temperature dynamics and actuation delays, have been considered for a better characterization of on-road platoon operating scenarios. To effectively incorporate the actual road and loading conditions,

an adaptive estimator has been included in the overall framework to estimate the road gradient and HCRV mass. Through numerical simulations, the proposed string stability controller incorporating brake fade dynamics and adaptive estimation scheme has been tested for different loading and road conditions and found to be delivering satisfactory performance in downgrade roads. The significant observations from this study are as follows:

1) If one were to opt for a conventional string stable controller design without opting for a brake fade compensated design, then it may result in collisions and subsequent loss in platoon stability while operating in downgrade roads.
2) The adaptive estimation scheme was needed to estimate the road gradient and HCRV mass accurately, without which maintaining a string stable operation was difficult, specifically in heterogeneous loading scenarios. The torque compensation provided by the controller depends on factors, viz., temperature developed, HCRV mass and road gradient, and a proper estimation of mass and road gradient was found to be necessary for the controller design to counter the brake fade effect and to ensure a string stable operation.
3) Overloading has a direct impact on platoon stability on downgrade roads. For an HCRV operating in 40% overloaded condition, the brake temperature developed was found to be 34% higher than that of a fully laden scenario, and this resulted in a further 18% reduction in the brake efficiency.
4) The adaptive estimation algorithm was found to be effective for slip values less than 0.5 depending on the road friction coefficient and deceleration magnitude. Beyond this value, the estimation algorithm fails to converge due to the discrepancies in the value of $F_x(t)$ calculated using brake pressure measurements.

The analysis carried out in this paper would be essential for realizing long-haul autonomous HCRV platoons. The key points addressed in this paper would help design a fault-tolerant string stable controller for the same. Potential stability issues during the reaching phase of the SMC operation need to be investigated. Addressing this issue would be considered as the immediate future scope of the presented work.

REFERENCES

[1] A. Alam, B. Besselink, V. Turri, J. Mårtensson, and K. H. Johansson, "Heavy-duty vehicle platooning for sustainable freight transportation: A cooperative method to enhance safety and efficiency," *IEEE Control Syst. Mag.*, vol. 35, no. 6, pp. 34–56, Dec. 2015.

[2] S. Sivanandham and M. Gajanand, "Platooning for sustainable freight transportation: An adoptable practice in the near future?" *Transp. Rev.*, vol. 40, no. 5, pp. 581–606, 2020.

[3] V. Milanés and S. E. Shladover, "Modeling cooperative and autonomous adaptive cruise control dynamic responses using experimental data," *Transp. Res. C, Emerg. Technol.*, vol. 48, pp. 285–300, Nov. 2014.

[4] M. Shang and R. E. Stern, "Impacts of commercially available adaptive cruise control vehicles on highway stability and throughput," *Transp. Res. C, Emerg. Technol.*, vol. 122, Jan. 2021, Art. no. 102897.

[5] D. Jia and D. Ngoduy, "Platoon based cooperative driving model with consideration of realistic inter-vehicle communication," *Transp. Res. C, Emerg. Technol.*, vol. 68, pp. 245–264, Sep. 2016.

[6] S. Maiti, S. Winter, and L. Kulik, "A conceptualization of vehicle platoons and platoon operations," *Transp. Res. C, Emerg. Technol.*, vol. 80, pp. 1–19, Jul. 2017.

[7] L. Zhang and G. Guo, "Control of connected vehicles with event-triggered transmission and prescribed energy budget," *J. Franklin Inst.*, vol. 358, no. 7, pp. 3651–3677, May 2021.

[8] C. Chen, J. Jiang, N. Lv, and S. Li, "An intelligent path planning scheme of autonomous vehicles platoon using deep reinforcement learning on network edge," *IEEE Access*, vol. 8, pp. 99059–99069, 2020.

[9] K. B. Devika, G. Rohith, and S. C. Subramanian, "Potential function-based string stable controller for heavy road vehicle platoons," *IEEE Access*, vol. 9, pp. 156274–156282, 2021.

[10] A. Tuchner and J. Haddad, "Vehicle platoon formation using interpolating control: A laboratory experimental analysis," *Transp. Res. C, Emerg. Technol.*, vol. 84, pp. 21–47, Nov. 2017.

[11] L. Xiao and F. Gao, "Practical string stability of platoon of adaptive cruise control vehicles," *IEEE Trans. Intell. Transp. Syst.*, vol. 12, no. 4, pp. 1184–1194, Dec. 2011.

[12] K. Liang, J. Mårtensson, and K. H. Johansson, "Heavy-duty vehicle platoon formation for fuel efficiency," *IEEE Trans. Intell. Transp. Syst.*, vol. 17, no. 4, pp. 1051–1061, Apr. 2015.

[13] B. Németh and P. Gáspár, "Optimised speed profile design of a vehicle platoon considering road inclinations," *IET Intell. Transp. Syst.*, vol. 8, no. 3, pp. 200–208, May 2014.

[14] K. Yu, H. Yang, X. Tan, T. Kawabe, Y. Guo, Q. Liang, Z. Fu, and Z. Zheng, "Model predictive control for hybrid electric vehicle platooning using slope information," *IEEE Trans. Intell. Transp. Syst.*, vol. 17, no. 7, pp. 1894–1909, Jul. 2016.

[15] B. Németh and P. Gáspár, "LPV-based control design of vehicle platoon considering road inclinations," *IFAC Proc. Volumes*, vol. 44, no. 1, pp. 3837–3842, Jan. 2011.

[16] C. Zhai, F. Luo, and Y. Liu, "Cooperative look-ahead control of vehicle platoon travelling on a road with varying slopes," *IET Intell. Transp. Syst.*, vol. 13, no. 2, pp. 376–384, Feb. 2018.

[17] D. Chen, S. Ahn, M. Chitturi, and D. Noyce, "Truck platooning on uphill grades under cooperative adaptive cruise control (CACC)," *Transp. Res. C, Emerg. Technol.*, vol. 94, pp. 50–66, Sep. 2018.

[18] J. Ploeg, D. P. Shukla, N. van de Wouw, and H. Nijmeijer, "Controller synthesis for string stability of vehicle platoons," *IEEE Trans. Intell. Transp. Syst.*, vol. 15, no. 2, pp. 854–865, Apr. 2013.

[19] X. Guo, J. Wang, F. Liao, and R. S. H. Teo, "Distributed adaptive integrated-sliding-mode controller synthesis for string stability of vehicle platoons," *IEEE Trans. Intell. Transp. Syst.*, vol. 17, no. 9, pp. 2419–2429, Sep. 2016.

[20] W. B. Dunbar and D. S. Caveney, "Distributed receding horizon control of vehicle platoons: Stability and string stability," *IEEE Trans. Autom. Control*, vol. 57, no. 3, pp. 620–633, Mar. 2011.

[21] G. Guo and D. Li, "Adaptive sliding mode control of vehicular platoons with prescribed tracking performance," *IEEE Trans. Veh. Technol.*, vol. 68, no. 8, pp. 7511–7520, Aug. 2019.

[22] K. B. Devika, R. G., V. R. Shreya Yellapantula, and S. C. Subramanian, "A dynamics-based adaptive string stable controller for connected heavy road vehicle platoon safety," *IEEE Access*, vol. 8, pp. 209886–209903, 2020.

[23] R. Limpert, *Brake Design and Safety*. Warrendale, PA, USA: SAE, 2011.

[24] J. Larson, K.-Y. Liang, and K. H. Johansson, "A distributed framework for coordinated heavy-duty vehicle platooning," *IEEE Trans. Intell. Transp. Syst.*, vol. 16, no. 1, pp. 419–429, Feb. 2014.

[25] A. Vahidi, A. Stefanopoulou, and H. Peng, "Recursive least squares with forgetting for online estimation of vehicle mass and road grade: Theory and experiments," *Vehicle Syst. Dyn.*, vol. 43, no. 1, pp. 31–55, 2005.

[26] J. Yang, J. Na, Y. Guo, and X. Wu, "Adaptive estimation of road gradient and vehicle parameters for vehicular systems," *IET Control Theory Appl.*, vol. 9, no. 6, pp. 935–943, Apr. 2015.

[27] H. Pacejka, *Tire and Vehicle Dynamics*. Amsterdam, The Netherlands: Elsevier, 2005.

[28] *IPG Truckmaker Reference Manual Version 7.0*, IPG Automot., Karlsruhe, Germany, 2018.

[29] R. Rajamani, *Vehicle Dynamics and Control*. Cham, Switzerland: Springer, 2011.

[30] N. Sridhar, K. V. Subramaniyam, S. C. Subramanian, G. Vivekanandan, and S. Sivaram, "Model based control of heavy road vehicle brakes for active safety applications," in *Proc. 14th IEEE India Council Int. Conf. (INDICON)*, Dec. 2017, pp. 1–6.
[31] K. Devika, N. Sridhar, H. Patil, and S. C. Subramanian, "Delay compensated pneumatic brake controller for heavy road vehicle active safety systems," *Proc. Inst. Mech. Eng. C, J. Mech. Eng. Sci.*, vol. 235, no. 13, pp. 2333–2346, Jul. 2021.
[32] F. Talati and S. Jalalifar, "Analysis of heat conduction in a disk brake system," *Heat Mass Transf.*, vol. 45, no. 8, p. 1047, 2009.
[33] D. Majcherczak, P. Dufreńoy, and M. Naït-Abdelaziz, "Third body influence on thermal friction contact problems: Application to braking," *J. Tribol.*, vol. 127, no. 1, pp. 89–95, Jan. 2005.
[34] V. Rajaram and S. C. Subramanian, "Design and hardware-in-loop implementation of collision avoidance algorithms for heavy commercial road vehicles," *Vehicle Syst. Dyn.*, vol. 54, no. 7, pp. 871–901, 2016.
[35] A. Alam, B. Besselink, V. Turri, J. Mårtensson, and K. H. Johansson, *Automotive Control Systems for Engine, Driveline, and Vehicle*. Berlin, Germany: Springer-Verlag, 2005.
[36] L. Chu, J. Gu, M. Liu, J. Li, Y. Gao, and M. Ehsani, "Study on CAN communication of EBS and braking performance test for commercial vehicle," in *Proc. IEEE Vehicle Power Propuls. Conf.*, Sep. 2007, pp. 849–852.
[37] H. Wilmar, "Improving the response of a wheel speed sensor by using a RLS lattice algorithm," *Sensors*, vol. 6, no. 2, pp. 64–79, Feb. 2006.
[38] K. B. Devika, G. Rohith, and S. C. Subramanian, "String stable control of electric heavy vehicle platoon with varying battery pack locations," *J. Vib. Control*, vol. 28, nos. 5–6, pp. 577–592, Mar. 2022.
[39] K. B. Devika and S. Thomas, "Power rate exponential reaching law for enhanced performance of sliding mode control," *Int. J. Control Automat. Syst.*, vol. 15, no. 6, pp. 2636–2645, Dec. 2017.
[40] M. W. Hancock and B. Wright, *A Policy on Geometric Design of Highways and Streets*. Washington, DC, USA: American Association of State Highway and Transportation Officials, 2013.
[41] L.-Y. Hao and G.-H. Yang, "Fault-tolerant control via sliding-mode output feedback for uncertain linear systems with quantisation," *IET Control Theory Appl.*, vol. 7, no. 16, pp. 1992–2006, 2013.
[42] B. Zheng, G. Yang, and T. Li, "Quantised feedback sliding mode control of linear uncertain systems," *IET Control Theory Appl.*, vol. 8, no. 7, pp. 479–487, May 2014.
[43] H. Chehardoli and A. Ghasemi, "Adaptive centralized/decentralized control and identification of 1-D heterogeneous vehicular platoons based on constant time headway policy," *IEEE Trans. Intell. Transp. Syst.*, vol. 19, no. 10, pp. 3376–3386, Oct. 2018.
[44] H. Chehardoli and A. Ghasemi, "Robust adaptive consensus of decentralized large-scale bi-directional vehicular platoons with only relative position measurement," *IEEE Trans. Veh. Technol.*, vol. 71, no. 2, pp. 1363–1371, Feb. 2021.
[45] L. An and G.-H. Yang, "Collisions-free distributed optimal coordination for multiple Euler-Lagrangian systems," *IEEE Trans. Autom. Control*, vol. 67, no. 1, pp. 460–467, Jan. 2021.
[46] R. Zhang, K. Li, Y. Wu, D. Zhao, Z. Lv, F. Li, X. Chen, Z. Qiu, and F. Yu, "A multi-vehicle longitudinal trajectory collision avoidance strategy using AEBS with vehicle-infrastructure communication," *IEEE Trans. Veh. Technol.*, vol. 71, no. 2, pp. 1253–1266, Feb. 2021.
[47] L. An and G.-H. Yang, "Distributed optimal coordination for heterogeneous linear multi-agent systems," *IEEE Trans. Autom. Control*, early access, Dec. 7, 2021, doi: 10.1109/TAC.2021.3133269.

K. B. DEVIKA received the Ph.D. degree in control systems from the National Institute of Technology, Calicut, India. She is a Lecturer in mechanical engineering with the College of Engineering, Mathematics and Physical Sciences, University of Exeter, U.K. Her research interests include control of automotive and transportation systems, clean mobility, and sliding mode control.

G. ROHITH received the Ph.D. degree in aerospace engineering from the IIT Madras, India. He is a Control Systems Engineer with Orbital Astronautics, Oxfordshire, U.K. His research interests include dynamics and control of automotive and aerospace systems and satellite attitude determination and control.

SHANKAR C. SUBRAMANIAN (Senior Member, IEEE) received the Ph.D. degree from Texas A&M University, USA. He is currently a Professor and V. Ramamurti Faculty Fellow with the Department of Engineering Design, IIT Madras, Chennai, India. His research interests include dynamics and control with applications to automotive and transportation systems.